Tectonics

RESEARCH ARTICLE
10.1029/2020TC006409

Key Points:
- The drag force induced by subduction direction reversal can invoke the continental breakup at continental convergent margins
- Continental interior and edge breakup modes develop depending on the "maturity" of the convergent margins and the oceanic lithosphere age
- Variation in the northwest-directed subduction of the PSCS is a reason breaking the relic arc and forearc along the strike of the SCS margin

Supporting Information:
- Supporting Information S1

Correspondence to:
F. Li and Z. Sun,
iamlifucheng@163.com;
zhensun@scsio.ac.cn

Citation:
Li, F., Sun, Z., Yang, H., Lin, J., Stock, J. M., Zhao, Z., et al. (2020). Continental interior and edge breakup at convergent margins induced by subduction direction reversal: A numerical modeling study applied to the South China Sea margin. *Tectonics*, *39*, e2020TC006409. https://doi.org/10.1029/2020TC006409

Received 2 JUL 2020
Accepted 29 SEP 2020
Accepted article online 6 OCT 2020

Continental Interior and Edge Breakup at Convergent Margins Induced by Subduction Direction Reversal: A Numerical Modeling Study Applied to the South China Sea Margin

Fucheng Li[1,2,3], Zhen Sun[1,2,3], Hongfeng Yang[4], Jian Lin[1,2,3,5], Joann M. Stock[6], Zhongxian Zhao[1,2,3], Hehua Xu[1,2,3], and Longtao Sun[1,2,3]

[1]CAS Key Laboratory of Ocean and Marginal Sea Geology, South China Sea Institute of Oceanology, Guangzhou, China, [2]Southern Marine Science and Engineering Guangdong Laboratory (Guangzhou), Guangzhou, China, [3]Innovation Academy of South China Sea Ecology and Environmental Engineering, Chinese Academy of Sciences, Guangzhou, China, [4]Earth System Science Programme, Faculty of Science, The Chinese University of Hong Kong, Hong Kong, [5]Department of Geology and Geophysics, Woods Hole Oceanographic Institution, Woods Hole, MA, USA, [6]Division of Geological and Planetary Sciences, California Institute of Technology, Pasadena, CA, USA

Abstract The dynamics of continental breakup at convergent margins has been described as the results of backarc opening caused by slab rollback or drag force induced by subduction direction reversal. Although the rollback hypothesis has been intensively studied, our understanding of the consequence of subduction direction reversal remains limited. Using thermo-mechanical modeling based on constraints from the South China Sea (SCS) region, we investigate how subduction direction reversal controls the breakup of convergent margins. The numerical results show that two distinct breakup modes, namely, continental interior and edge breakup ("edge" refers to continent above the plate boundary interface), may develop depending on the "maturity" of the convergent margin and the age of the oceanic lithosphere. For a slab age of ~15 to ~45 Ma, increasing the duration of subduction promotes the continental interior breakup mode, where a large block of the continental material is separated from the overriding plate. In contrast, the continental edge breakup mode develops when the subduction is a short-duration event, and in this mode, a wide zone of less continuous continental fragments and tearing of the subducted slab occur. These two modes are consistent with the interior (relic late Mesozoic arc) and edge (relic forearc) rifting characteristics in the western and eastern SCS margin, suggesting that variation in the northwest-directed subduction duration of the Proto-SCS might be a reason for the differential breakup locus along the strike of the SCS margin. Besides, a two-segment trench associated with the northwest-directed subduction is implied in the present-day SCS region.

1. Introduction

The South China Sea (SCS) is a typical extensional marginal sea basin similar to those found throughout the western Pacific. Despite structural similarities, the SCS also exhibits several distinctive features, for example, along-strike variation in the breakup locus (e.g., Briais et al., 1993; Cullen et al., 2010; Ding & Li, 2016; Franke et al., 2014; Huchon et al., 2001; Li et al., 2012). It is generally believed that before the opening of the SCS, a late Mesozoic ancient subduction zone existed along the SCS margin (e.g., Li & Li, 2007; Li, Sun, & Yang, 2018; Li, Suo, et al., 2019; Xia & Zhao, 2014; Xu et al., 2016; Ye et al., 2018). By recognizing the imprint of the late Mesozoic arc on the present-day SCS margin using petrological evidence and magnetic anomaly, Li, Sun, and Yang (2018) further inferred that the Cenozoic opening of the SCS basin broke the relic arc region (now continental interior) in the west and the relic forearc region (now continental edge) in the east (Figure 1a). In the west, the Dangerous Grounds block (Nansha block), which has an average crust thickness of ~24 km and width of >~400 km (Figure 1b), was separated from South China and migrated southward to Borneo during 25–20.5 Ma (Barckhausen et al., 2014; Qiu et al., 2011). In contrast, the opening of the SCS in the east occurred at the thin continental edge (Figure 1c), and as a result, the frontal part of the edge was split from the main continent and drifted southward since the Oligocene, finally forming the north Palawan (Holloway, 1982; Li, Sun, & Yang, 2018; Maruyama et al., 1997; Wang et al., 2019;

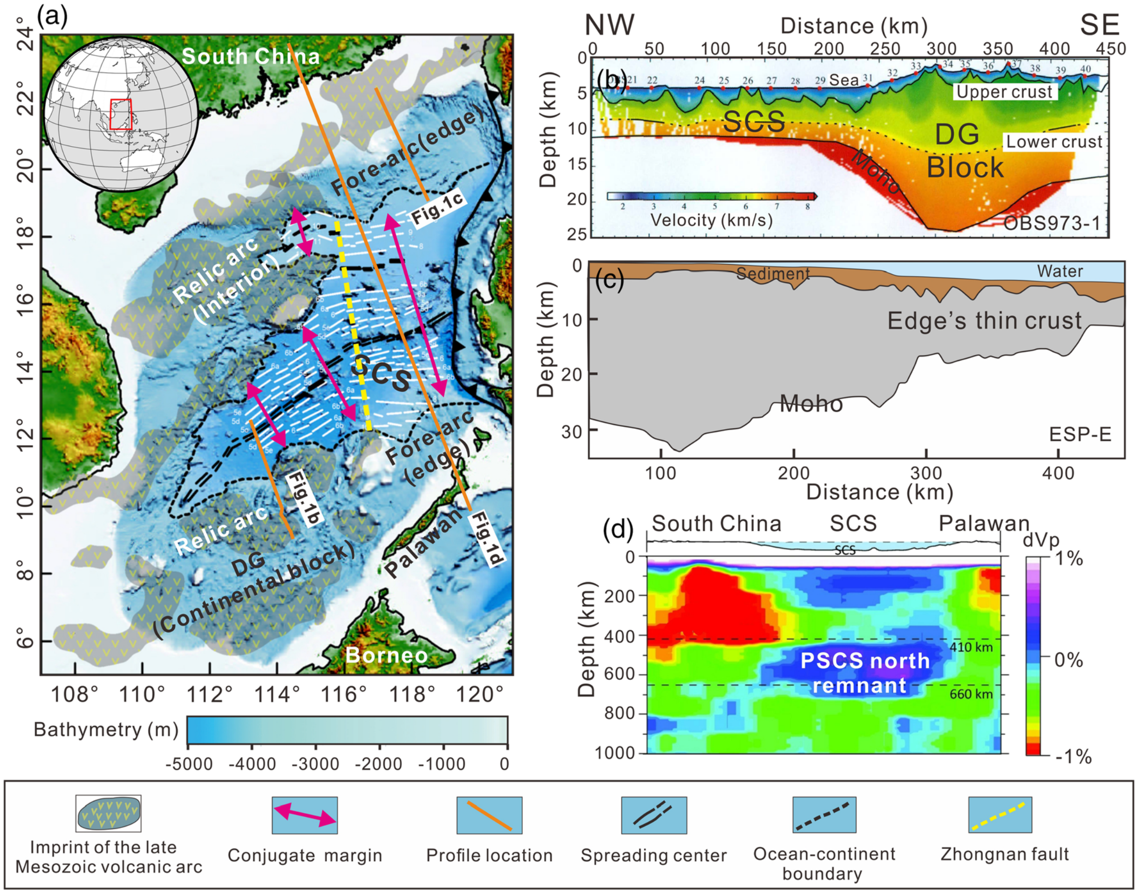

Figure 1. Observations in the South China Sea region. (a) Bathymetry map and the imprint of the late Mesozoic volcanic arc in the SCS region. The imprint of the late Mesozoic volcanic arc shows that the Cenozoic opening of the SCS basins has broken the continental interior in the west and the continental edge in the east (Li, Sun, & Yang, 2018). (b and c) Crustal velocity structures beneath the southwestern and northeastern margin (Nissen et al., 1995; Qiu et al., 2011). For more crustal structures in SCS, please refer to OBS2001 in Zhao et al. (2010) and OBS2006 in Wei et al. (2011). (d) Tomographic section indicating a subhorizontal fast slab anomaly (the PSCS north slab) under the east SCS (Sun et al., 2019; Wu & Suppe, 2018). DG: Dangerous Grounds (Nansha).

Zamoras & Matsuoka, 2004; Zhang et al., 2020; Zhao et al., 2020). Petrological analyses of sedimentary rocks revealed a forearc-related origin of the north Palawan, which was filled by subduction–accretion complexes and juxtaposed chert-clastic sequences in an imbricate manner (Isozaki, 1988; Marquez et al., 2006; Tumanda, 1991). Another remarkable feature of the eastern SCS region is slab tearing. Many recent tomographic studies showed that an oceanic slab remnant (referred to as the Proto-SCS [PSCS] north slab) existed in the east, lying within the asthenosphere of the SCS and exhibiting a fast *P* wave velocity anomaly (Figure 1d) (e.g., Hall & Spakman, 2015; Huang et al., 2015; Wu & Suppe, 2018; Zahirovic et al., 2016). A similar but smaller slab remnant was also recognized by interpreting the wide-angle seismic profiles (Zhou et al., 2006). These slab remnants were possibly the results of a slab-tear event that occurred during the rifting of the continental edge (Sun et al., 2019; Wu & Suppe, 2018).

Previous studies have investigated the causes of continental rifting through analyzing geological records, geophysical data, and modeling results (e.g., Bercovici, 2003; Buck, 1991; Coltice et al., 2019; Mohn et al., 2012; Nirrengarten et al., 2018; Péron-Pinvidic & Manatschal, 2009; Turcotte et al., 1983). Some of their end-members emphasized the role of plume-lithospheric interaction (e.g., Behn et al., 2004; Cande & Stegman, 2011; Husson, 2012; Jolivet et al., 2018; Koptev et al., 2015, 2019; Mondy et al., 2018; Phillips & Bunge, 2005; Yamato et al., 2013; Yoshida & Hamano, 2015), while others related the continental rifting to the tensional stresses generated at the plate boundary (e.g., Choi et al., 2013; Huismans & Beaumont, 2003; Le Pourhiet et al., 2018; Liao et al., 2013; Marotta et al., 2009; Naliboff et al., 2017; Pérez-Gussinyé et al., 2006). A series of numerical modeling studies further showed that, in both situations, tectonic loading, rollback process, preexisting weak structure, extension rate, crustal rheology, subduction depth, and thermal structure can control the first-order patterns of continental breakup (e.g., Burov & Watts, 2006; Dal Zilio et al., 2017; Duclaux et al., 2019; Gueydan & Précigout, 2014; Lavier & Manatschal, 2006; Nemčok et al., 2013; Pérez-Gussinyé et al., 2003; Ros et al., 2017; Svartman Dias et al., 2015; Tetreault & Buiter, 2018). Among these factors, slab rollback is the common dynamics of continental rifting at convergent margins (e.g., Heuret & Lallemand, 2005; Leng & Gurnis, 2011; Sdrolias & Muller, 2006; Stern, 2002). For example, most of the marginal basins in the western Pacific, such as the Mariana Trough and Okhotsk Basin, have been considered as backarc basins associated with the rollback process that took place along the trenches, where the Pacific and the Eurasian plates converge (Karig, 1971). During rollback subduction, the rifting features may be different by considering the slab-slab interactions (e.g., Faccenna et al., 2018; Holt et al., 2018; Mishin et al., 2008), trench migration rates (e.g., Becker et al., 2015), plate properties (e.g., Capitanio et al., 2010; Crameri & Tackley, 2015; Rodríguez-González et al., 2012), subduction erosion (e.g., Keppie et al., 2009; Von Huene & Scholl, 1991), and plate velocities (e.g., Wolf & Huismans, 2019). These former studies focused solely on the consequence of slab rollback and emphasized its role in breaking the convergent margins. Less attention, however, has been paid to other mechanisms, such as drag-force caused by the subduction direction reversal that occurred in the SCS region.

In the widely accepted subduction-collision model, the opening of the SCS was viewed as a consequence of drag force associated with southeastward subduction of a proto-oceanic plate (usually called PSCS) underneath Borneo (e.g., Hall, 2002; Hutchison, 2004). The PSCS was believed to be oceanic crust which once occupied the area north of Borneo, wherein the present-day SCS is located (Figure 2a). The tectonic reconstruction revealed that the subduction of the PSCS started along the South China margin and later shifted toward the southeast in the Eocene (~45 Ma) (Hall, 2002; Wu & Suppe, 2018) (Figures 2c and 2d). The southeast-directed subduction invoked extension on the South China margin, which ultimately separated the Dangerous Grounds from the main continental body and created the SCS in between. The Dangerous Grounds was then dragged southward and finally collided with Borneo in the middle Miocene, which is regarded as the end of the PSCS subduction (e.g., Holloway, 1982) (Figures 1b and 2f). The remnant slabs of the PSCS (north and south) are now trapped in the asthenosphere beneath the South China and Palawan, respectively (Figure 2f) (Fan et al., 2017; Li, Sun, & Yang, 2018; Wu & Suppe, 2018). Although the geological processes have been discussed previously, there still lacks a quantitative test of this hypothesis. It remains unclear whether the subduction direction reversal can cause the continental breakup and, if so, how does this process break the continental edge or interior? Several numerical studies have been performed to investigate the formation of the SCS through modeling the lithospheric extension (e.g., Brune et al., 2016; Le Pourhiet et al., 2018; Li, Sun, et al., 2019), but their models focused mainly on rifting process without considering the role of subduction direction reversal. It is necessary to conduct a further study to improve our understanding of the rifting process in a convergent tectonic system.

Here we attempt to investigate the effects of subduction direction reversal on the development of continental breakup using a series of 2-D thermo-mechanical models. With these numerical models, we will also test the hypothesis that the "maturity" of convergent margins (in terms of subduction duration) and age of the oceanic lithosphere are crucial for explaining the contrasting breakup types along the strike of the SCS margin.

2. Numerical Model Description

The simulations in this study are performed using a 2-D thermo-mechanical code modified after Gerya (2010), solving the Stokes and heat transfer equations. More details about the governing equations, material parameters, and benchmarks used in the numerical experiments are in the supporting information and example of "viscoelastic-plastic subduction" in the reference book.

We design a model domain of 1,100 km × 500 km in the x and y dimensions with a nonuniform rectangular grid and randomly distributed markers. The Eulerian grid in the vicinity of the subduction zone has a higher resolution of 1 km × 1 km, whereas the rest of the model increases the grid spaces away from the high-resolution domain by a constant gradient of 1.1. In total, ~1.6 million random Lagrangian markers are evenly distributed in the Eulerian cells.

Our initial setup is a standard subduction model that consists of two parts: (1) an upper continental plate and (2) a subducting slab. The continental plate is composed of an upper crust and a lower crust with a total

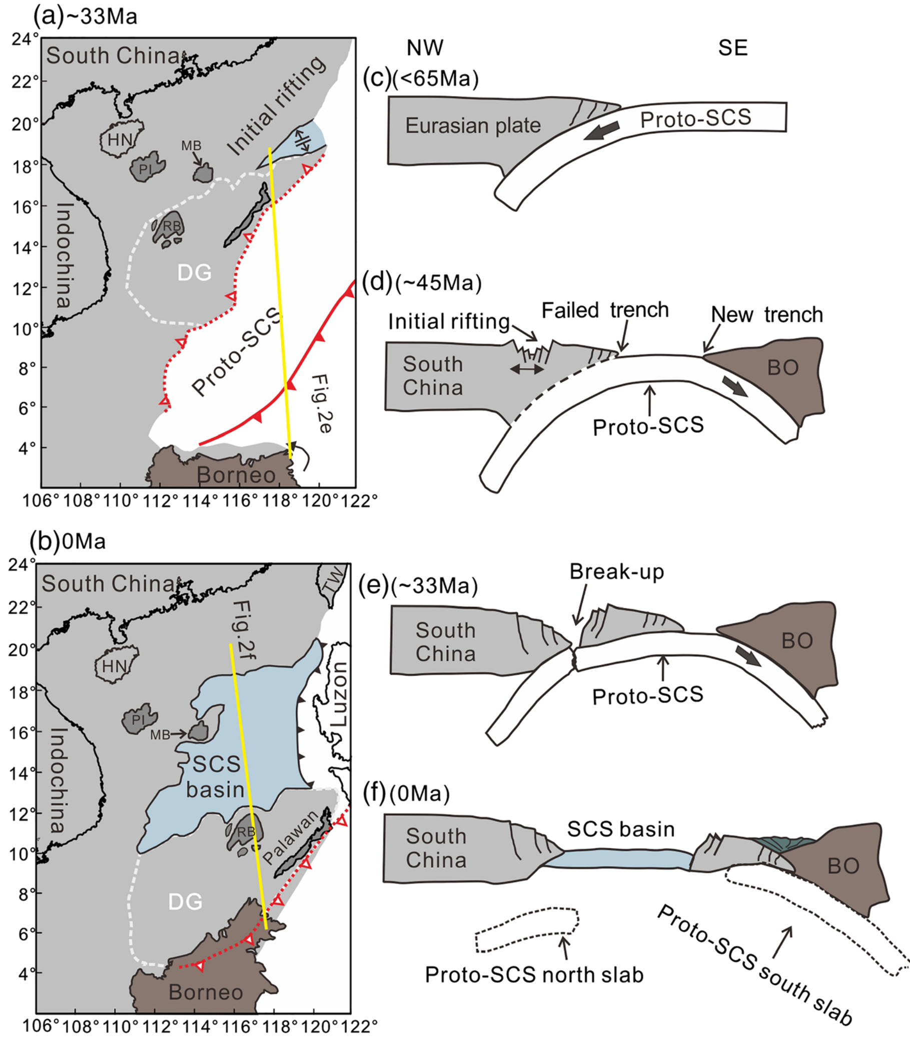

Figure 2. Plate reconstructions of the SCS region. The schematic of the process of subduction direction reversal in plane (a–b) and in profile (c–f) (summarized after Hall, 2002; Holloway, 1982; Li et al., 2014; Li, Sun, & Zhang, 2018; Pautot et al., 1986; Sun et al., 2009, 2019; Wu & Suppe, 2018). (HN: Hainan; MB: Zhongsha Bank [Macclesfield Bank]; PI: Xisha Islands [Paracel Islands]; RB: Reed Bank; BO: Borneo; DG: Nansha [Dangerous Grounds]; TW: Taiwan; PN: Palawan; SCS: South China Sea).

thickness of 35 km, underlain by lithospheric mantle up to a depth of 85 km that was estimated from a regional *S*-velocity model (Figures 3a and 3d) (An & Shi, 2006). Following earlier similar studies (e.g., Beaussier et al., 2019; Koptev et al., 2019; Liao & Gerya, 2017), the upper and lower continental crust in our numerical experiments are prescribed with quartzite and plagioclase rheology, respectively (Ranalli & Murphy, 1987; Shelton et al., 1981). The mantle is represented by dry olivine rheology, which is controlled by a combination of Power-law, diffusion, and Peierls creep (Chopra & Paterson, 1981; Durham et al., 2009; Karato & Wu, 1993; Kirby, 1983) (see supporting information). The oceanic crust is given by a 2-km-thick basalt-like oceanic upper crust and a 5-km-thick gabbro-like oceanic lower crust (e.g., Turcotte & Schubert, 2002) (Figure 3d). We describe the brittle behavior of rocks by the classical Mohr-Coulomb failure criterion (see, e.g., Vermeer, 1990). Strain softening is specified as a linear decrease of the friction angle with increasing accumulated strain (see, e.g., Gerya, 2010).

Statistical analyses of trenches in the western Pacific (Lallemand et al., 2005) and near-field seismic observations (Zhu et al., 2019) show an average slab dip of 28° at shallow depth (Figure 3b), so we initiate the subduction by prescribing a 28° dipping weak fracture zone between the continental and oceanic plates. This weak zone consists of mantle rocks with wet olivine rheology (Chopra & Paterson, 1981; Ranalli, 1995)

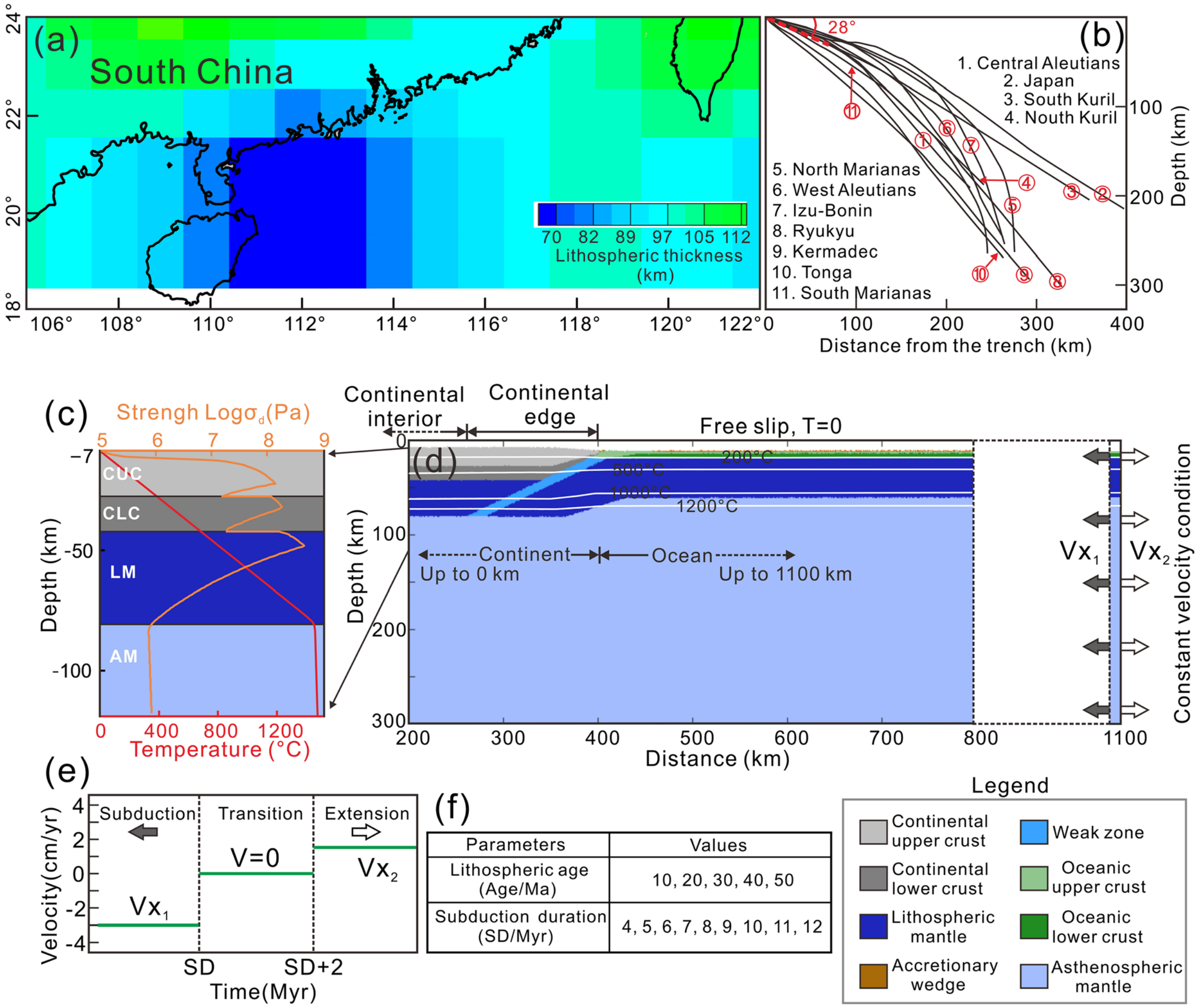

Figure 3. Initial model setup and constraints: (a) seismic-thermal lithosphere thickness of the South China block and surrounding SCS margin (An & Shi, 2006), (b) statistical analysis of subduction dips in the western Pacific (summarized after Lallemand et al., 2005), (c) yield strength profile (brown line) and geotherm (red line) of the continent, (d) enlarged 600 km × 300 km domain of the original 1,100 km × 300 km model (continental edge and interior in the modes depending on whether the continent directly overlies the plate boundary interface), (e) variable velocity boundary conditions on the right side of the model domain, (f) key variable parameters of the numerical experiments. CUC: continental upper crust; CLC: continental lower crust; LM: lithospheric mantle; AM: asthenospheric mantle.

and low plastic cohesion (1 MPa), thus facilitating the subduction along the channel (Figure 3d). A 7 km-thick "sticky air" ($\eta = 10^{18}$ Pa·s, $\rho = 1$ kg/m^3) layer is imposed on the model's upper surface to provide a free-surface-like condition that allows topographic evolution (Crameri et al., 2012). The details of the material parameters are illustrated in Table S1.

Our model has a constant temperature boundary condition at the top and bottom boundaries, while the left and right boundaries are thermally isolated. The initial thermal structure of the continental lithosphere increases vertically from 0°C at the surface to 1380°C at 85 km in a linear trend (Figure 3c). The initial temperature of the asthenosphere mantle increases with depth at a gradient of 0.5°C/km. The thermal structure of the oceanic plate is defined by a half-space cooling age (Turcotte & Schubert, 2002). However, the age of the PSCS is still in debate, and previous studies have argued that the PSCS was possibly a remnant of the Paleo-Pacific/Meso-Tethys, a Mesozoic oceanic embayment, a backarc basin, or a marginal basin (e.g., Holloway, 1982; Taylor & Hayes, 1983; Zhou et al., 2005). Therefore, we vary the ages of the oceanic lithosphere (e.g., 10, 20, 30, 40, and 50 Ma) to explore their potential effects (Figure 3f).

The mechanical boundary conditions are free slip at the top and left side boundaries. The bottom boundary is permeable in the vertical direction to satisfy an external/internal free slip boundary condition (Burg & Gerya, 2005). To represent the motion of the PSCS, we assign a constant convergence velocity followed by divergence velocity on the right side of the model domain. During the first 4 Myr (5 to 12 Myr also will be tested), we impose a constant convergence velocity of −3 cm/yr to initiate the leftward subduction (Figures 3d and 3e). To get a smooth transition from subduction to extension, we follow the approach of Jourdon et al. (2019), adopting a 2 Myr window between convergence and divergence to simulate a period of tectonic quiescence. That is, the velocity is zero from 4 to 6 Myr. Then, after 6 Myr, a constant divergence velocity of 1.5 cm/yr is prescribed on the right side until the end of the simulation (Figure 3e). More models are conducted by varying the subduction duration from 4 to 12 Myr to investigate the role of convergent margin "maturity" and hence that the subsequent extension starts at 6 to 14 Myr, respectively.

To differentiate the initial breakup locations, we divide the continental domain into two lithospheric units: the continental edge and interior, depending on whether the continent directly overlies the plate boundary interface (Figure 3d). The continental edge is above the interface with a thin and wedge-shaped lithosphere, while the continental interior is located adjacent to the continental edge and is characterized by a stable and larger lithospheric thickness than that of the continental edge.

3. Results

To test the hypotheses concerning the variable lithospheric age and subduction duration, several groups of numerical experiments are designed in this study. Each group includes a given lithospheric age and nine different subduction durations (4 to 12 Myr).

3.1. Group 1: Lithospheric Age of 10 Ma and Variable Subduction Duration

Group 1 has a lithospheric age of 10 Ma. The results with subduction duration of 4, 6, 8, and 10 Myr are selected in Figure 4 (Models 1–4). All these models experience a steady-state subduction process during convergent margin evolution, and the slabs finally reach different depths at the end of the subduction stage.

During lithospheric extension, these models display a similar first-order deformation behavior. Moreover, at the end of the extension, the initial breakup occurs at the continental edge that specifies the leading edge of the upper continent overlying the plate boundary interface. For example, as revealed by Model 1, the divergent velocity exerts a negligible effect on the continent at 6 Myr so that the continent is not involve in the extensional activity at the early stage of the lithospheric extension. At the same moment, the relative motion along the plate boundary interface accommodates almost the entire model's deformation (Figure 4a, at 6 Myr). At 12 Myr, the oceanic plate returns to a shallow depth. The intense strain localization begins to occur at the continental edge and propagates into the underlying oceanic lithosphere (Figure 4a, at 12 Myr). At 19 Myr, the continental edge eventually breaks into pieces along the shear zone. These newly formed continental fragments move together with the oceanic plate to the right side (Figure 4a, at 19 Myr). Another distinctive characteristic is the tearing of the subducted slab. Therefore, a slab remnant can be observed below the overriding continental plate at the end of the modeling (Figure 4a, at 19 Myr).

Also note that, in the long-period subduction cases (Models 3 and 4), the incipient breakup is delayed by ~9–15 Myr compared to that in the short-period subduction cases (Models 1 and 2). This addition time ultimately leads to the slab remnant sinking into the asthenosphere (Figure 4c, at 28 Myr and Figure 4d, at 34 Myr).

3.2. Group 2: Lithospheric Age of 20 Ma and Variable Subduction Duration

Group 2 has a lithospheric age of 20 Ma. We also select the models with subduction durations of 4, 6, 8, and 10 Myr for comparison (Figure 5, Models 5–8). The evolution of models in Group 2 becomes quite different when the tectonic inversion starts. The major part of the strain localizes in the continental edge and the oceanic slab (Models 5–7) or in the continental interior (Model 8), depending on the subduction duration. As a result, two distinct continental breakup modes, namely, continental edge and interior breakup, develop at the end of the experiment.

Similar to the results in Group 1, Models 5–7 exhibit the rift features of the continental edge breakup mode, for example, relative motion between the plates, tearing of the subducted slab, and formation of the

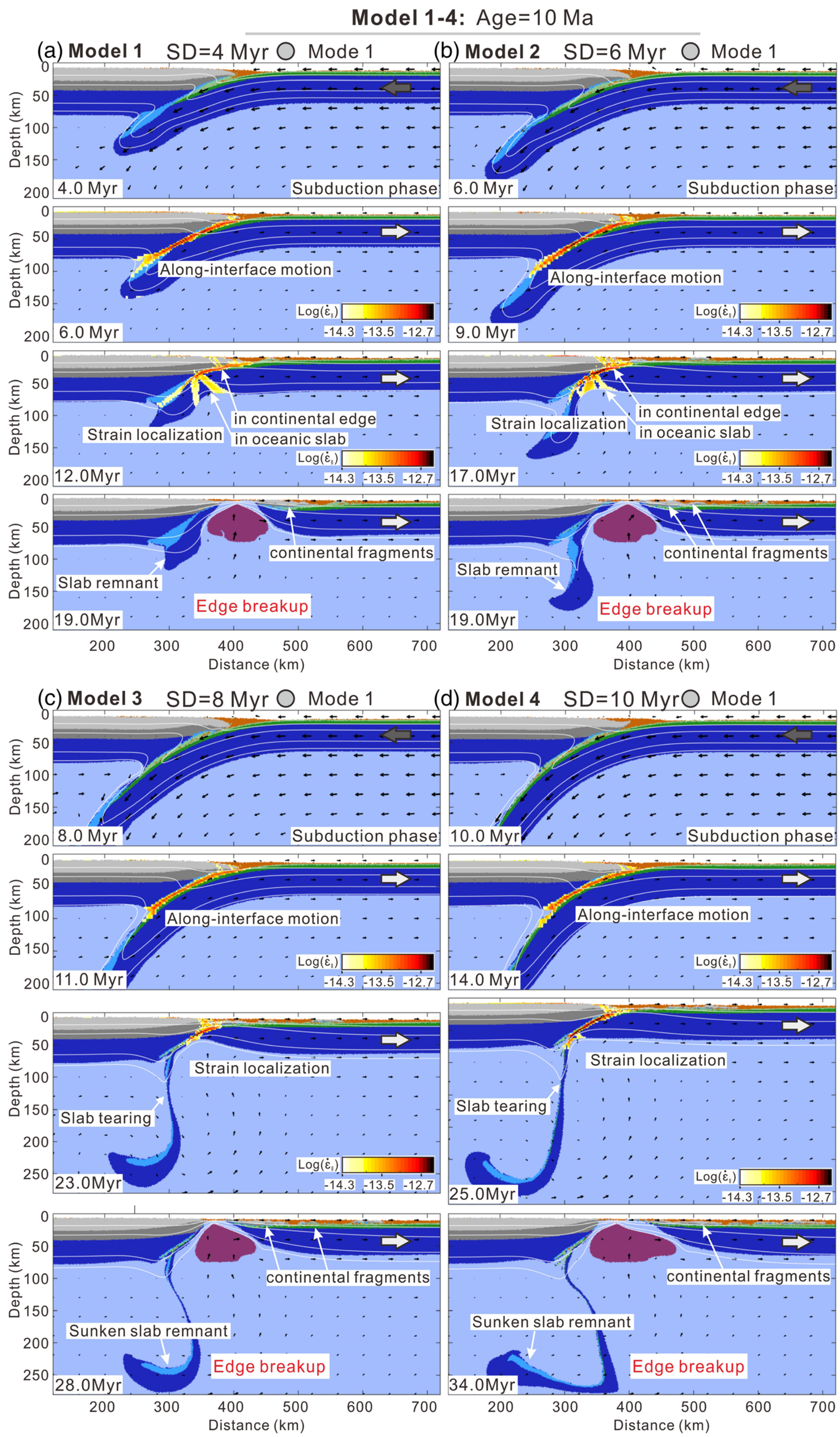

Figure 4. Evolution of Group 1. Oceanic lithospheric age of 10 Ma and subduction duration (SD) of (a) 4 (Model 1), (b) 6 (Model 2), (c) 8 (Model 3), and (d) 10 Myr (Model 4). The inset colors show the second invariant of the strain rate (as in the color bar). White lines are isotherms in °C. Black arrows denote the calculated velocity field. The colors of rock types are as in Figure 2. Circle denotes the continental edge breakup mode.

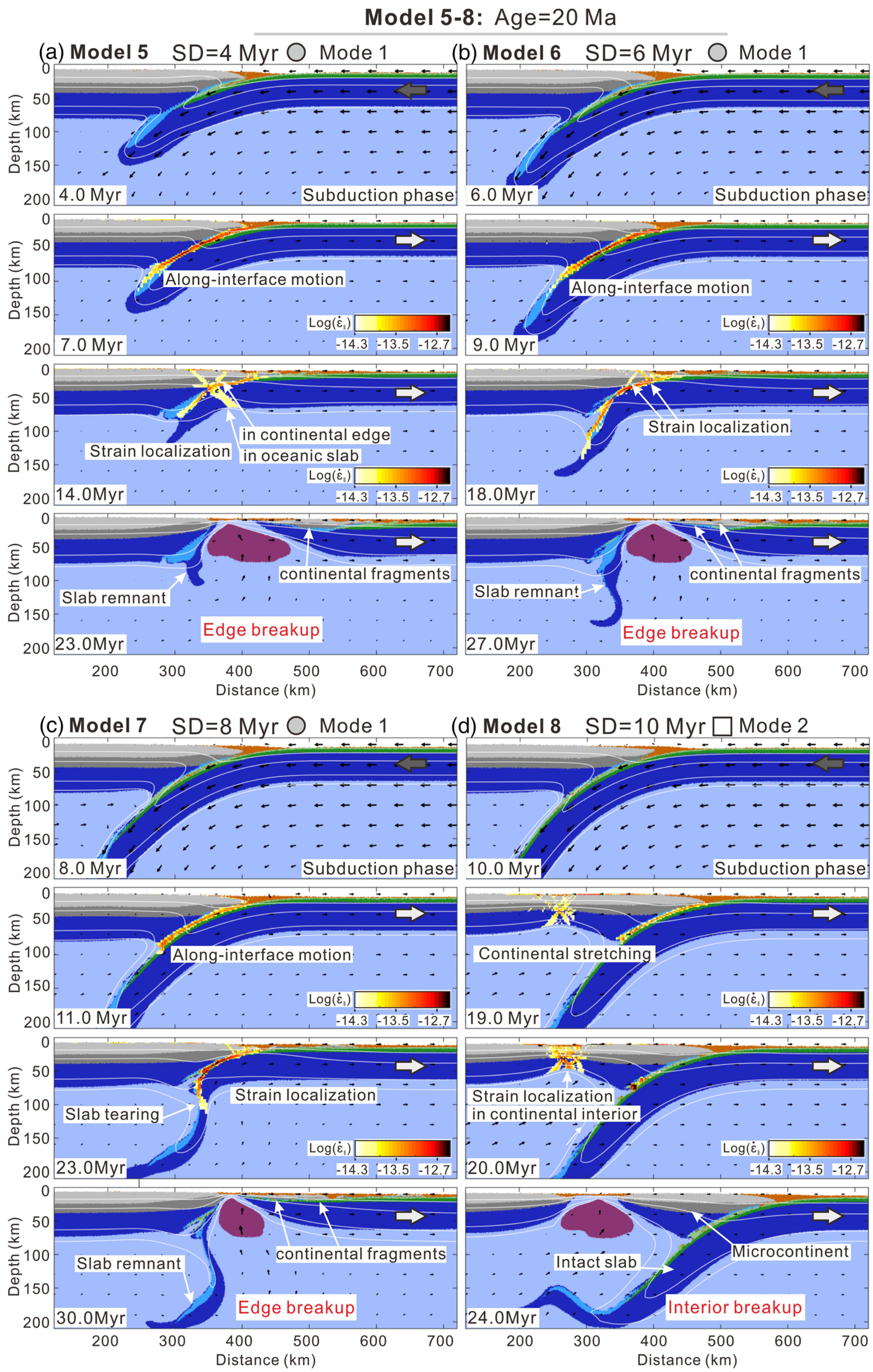

Figure 5. Evolution of Group 2. Oceanic lithospheric age of 20 Ma and subduction duration (SD) of (a) 4 (Model 5), (b) 6 (Model 6), (c) 8 (Model 7), and (d) 10 Myr (Model 8). The inset colors show the second invariant of the strain rate (as in the colorbar). White lines are isotherms in °C. Black arrows denote the calculated velocity field. The colors of rock types are as in Figure 2. Circle and square denote the continental edge and interior breakup mode, respectively.

continental fragments. In contrast, Model 8 shows another scenario in which no clear relative motion between the plates occurred during extension. Instead, the continent is subject to continuous stretching, and as a result, lithospheric-scale shear bands develop in the continental interior to accommodate most of the extensional strain (Figure 5d, at 20 Myr). Such differences possibly stem from that the slab in Model 8 has been subducted to greater depth, thus increasing the interplate contact area and exhibiting a strong plate coupling during the rifting stage. As extension progresses, the continent extends over a large scale and develops a typical necking in the lithospheric mantle, similar to those in previous studies (e.g., Chenin et al., 2017; Duretz et al., 2016; Li, Sun, et al., 2019). At the end of the system's development, breakup initiates in the continental interior, which is approximately 200 km away from the trench, separating a microcontinent from the main continent body. The microcontinent migrates rightward together with the oceanic plate, while the rest of the continent remains in its original location, forming a new passive margin (Figure 5d, at 24 Myr).

3.3. Group 3: Lithospheric Age of 30 Ma and Variable Subduction Duration

Group 3 has an oceanic age of 30 Ma. Figure 6 summarizes the evolution of models with subduction durations of 7, 8, 9, and 10 Myr. The essential features of this group are similar to Group 2. Group 3 also concludes that breakup can occur at the continental edge or within the interior, depending on the subduction duration.

It is also noteworthy that an increase in the lithospheric age can enhance the mechanical locking at the plate interface. Thus, compared to the earlier groups, Group 3 requires an even shorter subduction duration to facilitate the development of interior breakup. For example, in contrast to Group 2, where the model with a subduction duration of 6 Myr is characterized by continental edge breakup (Model 6), here the 6 Myr induces the breakup of the continental interior (Model 10, Figure 6b). This implies that, in the case of the oceanic age of 30 Ma, the continental edge breakup only occurs when the subduction ends earlier than 6 Myr (Figure 6a).

4. Discussion

4.1. Summary of Numerical Results

Our experiment results demonstrate that variations in the subduction duration when the reversal of subduction direction happened may result in two contrasting continental breakup modes at the end of the rifting stage. In general, short-period subduction duration shows a weak coupling condition, and, as a result, the relative motion along the plate boundary interface accommodates the model's deformation at the early extension stage. When the oceanic slab returns to a shallow depth, the deformation begins to localize at the continental edge and eventually breaks the continental edge (Figure 7b). In the edge breakup mode, the extension also tears the subducted oceanic slab into two plates. The main oceanic plate moves rightward, whereas the remnant is trapped beneath the continental lithosphere (Figure 7b). In contrast, the long-period subduction duration model exhibits a strong coupling between the subducting and overriding plates when the subduction direction reversal occurs. In these strongly coupled cases, deformation mainly localizes within the continent interior, which finally breaks up at the end of rifting (Figure 7c).

As shown in Figure 7d, we summarize the models in terms of breakup types as a function of subduction duration and age of the oceanic lithosphere. The results show that, for a given slab age of ~15 to ~45 Ma, the less the subduction duration is, the greater the likelihood of continental edge breakup will occur (shadow area in Figure 7d). For example, subduction duration should be less than 8 Myr to induce edge breakup for a slab age of 20 Ma; otherwise, the breakup will occur within the continental interior. Furthermore, as the slab age increases, the subduction duration required to induce the continental edge breakup is reduced. For example, the age of 20 Ma can promote the breakup of continental edge on the condition that the subduction ends earlier than 8 Myr, whereas the age of 30 Ma requires a subduction duration less than 4 Myr (shadow area in Figure 7d).

The results also suggest that, once the slab age exceeds ~45 Ma, the breakup of the continental edge has never been observed because the mechanical plate coupling is sufficiently strong to resist extension. Yet the continental edge breakup always occurs when the age is younger than ~15 Ma due to weak plate coupling (Figure 7d).

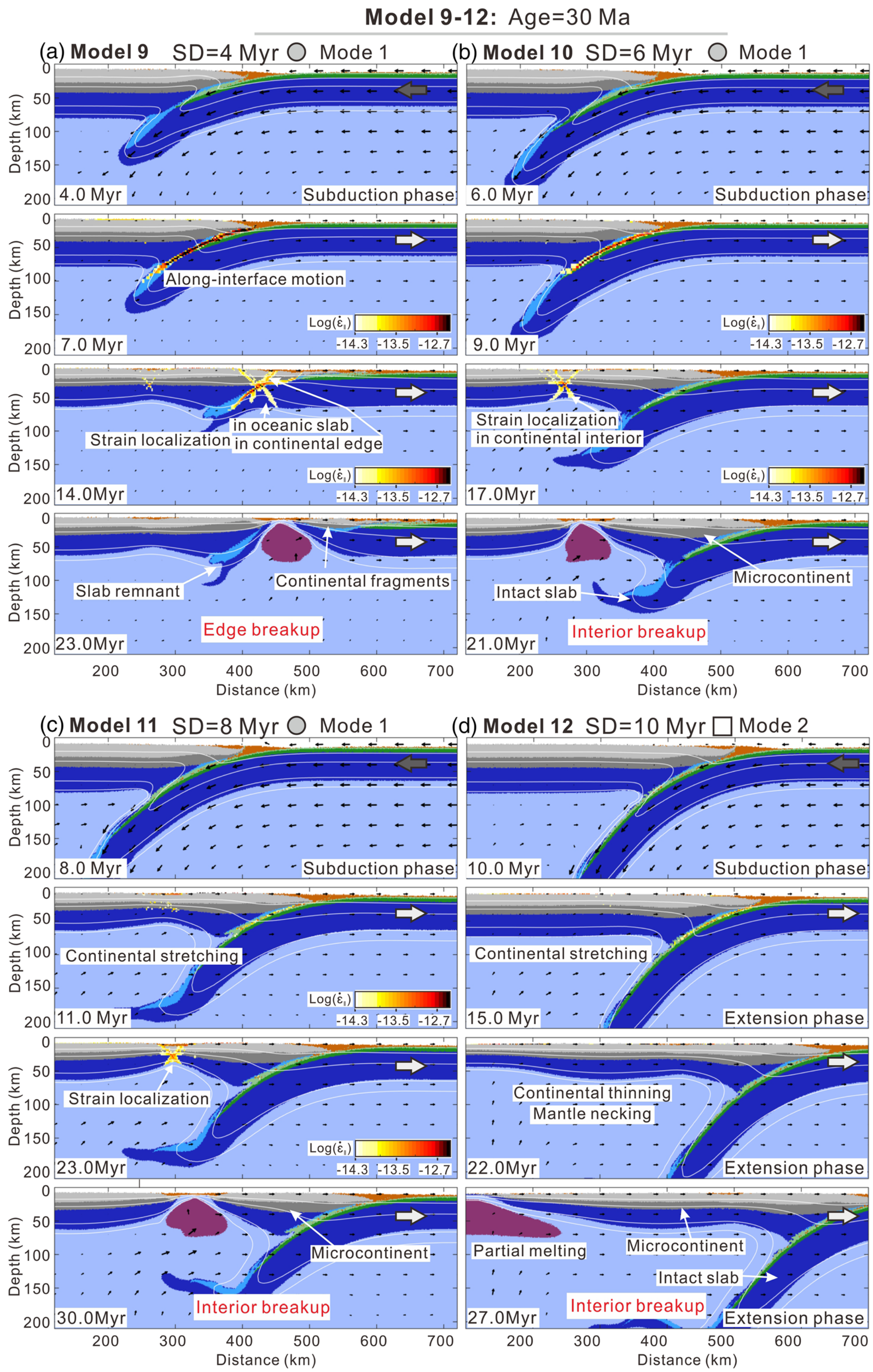

Figure 6. Evolution of Group 3. Oceanic lithospheric age of 30 Ma and subduction duration (SD) of (a) 4 (Model 9), (b) 6 (Model 10), (c) 8 (Model 11), and (d) 10 Myr (Model 12). The inset colors show the second invariant of the strain rate (as in the colorbar). White lines are isotherms in °C. Black arrows denote the calculated velocity field. The colors of rock types are as in Figure 2. Circle and square denote the continental edge and interior breakup mode, respectively.

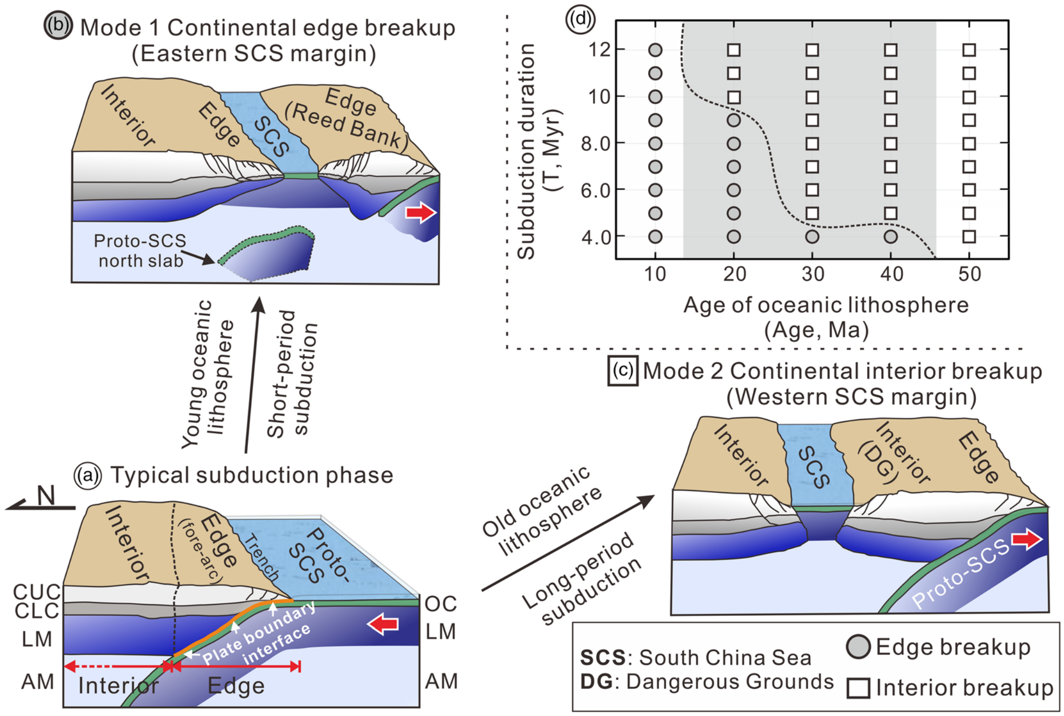

Figure 7. Conceptual models of the contrasting continental breakup modes (a–c) and area diagram summarizing the models in terms of breakup types as a function of subduction duration and age of the oceanic lithosphere (d). (a) Typical subduction zone, in which the upper plate is divided into continental edge and interior according to whether they are located directly above the slab-lithosphere interface. (b, c) Illustration of the breakup of the continental interior and edge, respectively. (d) The dashed line marks the threshold values indicating the transformation from continental edge to interior breakup. The shadow area denotes the conditions under which both breakup modes at a given age can be expected by varying the subduction duration. CUC: continental upper crust; CLC: continental lower crust; LM: lithospheric mantle; AM: asthenospheric mantle; OC: oceanic crust.

4.2. Models Consistent With Observations in the SCS Continental Margin

In the SCS continental margin, the relic Mesozoic volcanic arc was broken and extended over a wide area in the west, whereas the arc in the east is less extended and kept its original configuration (Li, Sun, & Yang, 2018). These observations are consistent with our numerical results. In the interior breakup mode, strain mainly localized further away from the trench and along the continental interior during extension. As extension proceeded, the arc may be stretched over a wide area and finally was split by the opening of the oceanic basin (Figure 7c). The western SCS margin followed the interior breakup mode and thus developed a wide range of arc in both conjugate margins of the southwestern subbasin. By contrast, the eastern SCS margin was ruptured along the relic forearc region, and, as a result, the late Mesozoic arc was rarely extended and was left on the Chinese side with its original configuration during the opening of the SCS basin. Another important characteristic in the east is that a portion of the PSCS slab lies under the present-day SCS and exhibits a high-velocity feature (Figure 1d) (Wu & Suppe, 2018). These aforementioned characteristics are in agreement with our continental edge mode, where the breakup occurred along the forearc region and was accompanied by the tearing of the subducted slab (Figure 7b).

By reconstructing the plate boundary between Sundaland and the Dangerous Grounds, Clift et al. (2008) proposed that the PSCS was about 1,000-km-wide in the north-south direction (Figure 8). Many previous studies believed that the PSCS has been subducted northwestward beneath the South China block and southeastward beneath the northern Borneo (Hall, 2002; Wu & Suppe, 2018) (Figure 2). The southeast dipping subduction goes in a scissor-like fashion, in which a larger portion of the oceanic plate has been subducted beneath Sarawak than beneath Sabah (Madon et al., 2013) (Figure 8). Therefore, the amount of the PSCS subducted beneath the South China block can be roughly estimated by subtracting the southeast subducted slab from the total width. The results shown in Figure 8 indicate that a larger portion of the

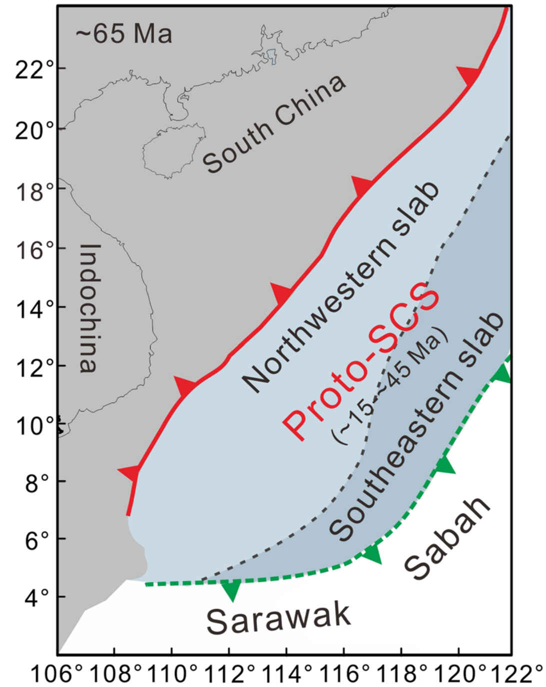

Figure 8. Sketch map showing the proportion of the Proto-SCS (PSCS) subducting toward the northwest and southeast with oceanic ages of ~15–45 Ma. In the northwest dipping subduction (red line), a larger portion of the PSCS has been subducted beneath the western South China margin compared to that beneath the eastern South China margin. The dashed line divides the PSCS into northwestern and southeastern slabs, which have been subducted beneath the South China block (along the red line) and Sarawak/Sabah (along the green line), respectively.

PSCS is subducted beneath the western South China margin than that beneath the eastern South China margin. In other words, the western South China margin experiences a longer period of subduction compared to the eastern margin.

The variation in the subduction duration has a good correspondence with the differential breakup characteristics along the strike of the South China margin. As shown in Figures 1 and 8, the eastern South China margin is characterized by the breakup of the edge region and experiences a relatively short period of the PSCS subduction. By contrast, the western margin has been broken within the interior and undergoes a relatively long period of subduction. These phenomena are consistent with our numerical results, where a long subduction duration induces the continental interior breakup, whereas a short duration causes the continental edge breakup. Therefore, our studies demonstrate that variation in the duration of northwest dipping subduction might be a cause for the contrasting breakup types along the strike of the SCS margin.

4.3. Model Implication for the Northwest-Directed Subduction Trench

Previous studies have revealed that the southeast-directed subduction trench locates at the southern SCS margin, but the northwest-directed subduction trench remains unclear. In combination with the numerical results and geophysical characteristics, this section will discuss the possible northwest-directed trench locations. As mentioned by previous studies (e.g., Zhou et al., 2008), the horizontal gradient of the Bouguer anomaly (HGBA) is sensitive to lateral material contrast and thus can illustrate the tectonic boundaries. In the HGBA map of the SCS region, a few high-amplitude anomaly belts are observed clearly parallel/subparallel to the margin (Figure 9a). We number these belts and find that many of them are well correlated with the known plate boundaries in the SCS region. For example, Belt 2 delineates the shape of the SCS oceanic basin, consistent with the continent-ocean boundaries. The Manila trench, where the SCS plate is subducting beneath the Philippine Sea plate, is delineated by the high-amplitude anomaly Belt 3.

Belt 4 is located at the southern end of the Nansha Trough (NW Borneo trough) and corresponds to a relic trench, also known as the thrust front that is related to the southeast-directed subduction of the PSCS beneath Borneo (Franke et al., 2008; Hamilton, 1979). The southeast-directed subduction ceased in the Early Miocene when the Dangerous Grounds collided with Borneo causing compressive deformation at the thrust front (e.g., Hall et al., 2008; Hutchison, 1996). As collision proceeded, the attenuated continental crust of the Dangerous Grounds went underneath Borneo. The southern Dangerous Grounds leading edge has been thrust beneath the Crocker-Palawan accretionary wedge, possibly as far to the onshore beneath Mount Kinabalu (MK in Figure 9a) in Borneo (e.g., Cottam et al., 2010; Cullen et al., 2010; Franke et al., 2008; Hutchison & Vijayan, 2010; Steuer et al., 2013). Belt 5 well crosses Mount Kinabalu and overlaps the regions of the Crocker-Palawan complex, thus possibly denoting the southern boundary of the Dangerous Grounds (Figure 9b). According to the evolution of our continental interior breakup mode, the Dangerous Grounds is separated from the main South China continent, and its southern boundary might be the site where the northwest-directed trench was ever located (Figure 9c).

We also note that a distinct belt (named Belt 1) in the northeastern SCS margin does not correspond to any known plate boundaries yet shows strong lateral material contrast, extending from the Central Uplift to the Yitongansha (Figure 9a). Integrating numerical results with observations, we infer the belt probably due to the existence of a slab remnant that is trapped beneath the continent during the continental edge breakup. The breakup of the continental edge tears the oceanic plate and causes the remnant staying in the subduction channel or sinking into the asthenosphere, thus causing a strong lateral material contrast (Figure 9c). Our interpretation is also supported by other independent evidence. For instance, a remnant of the

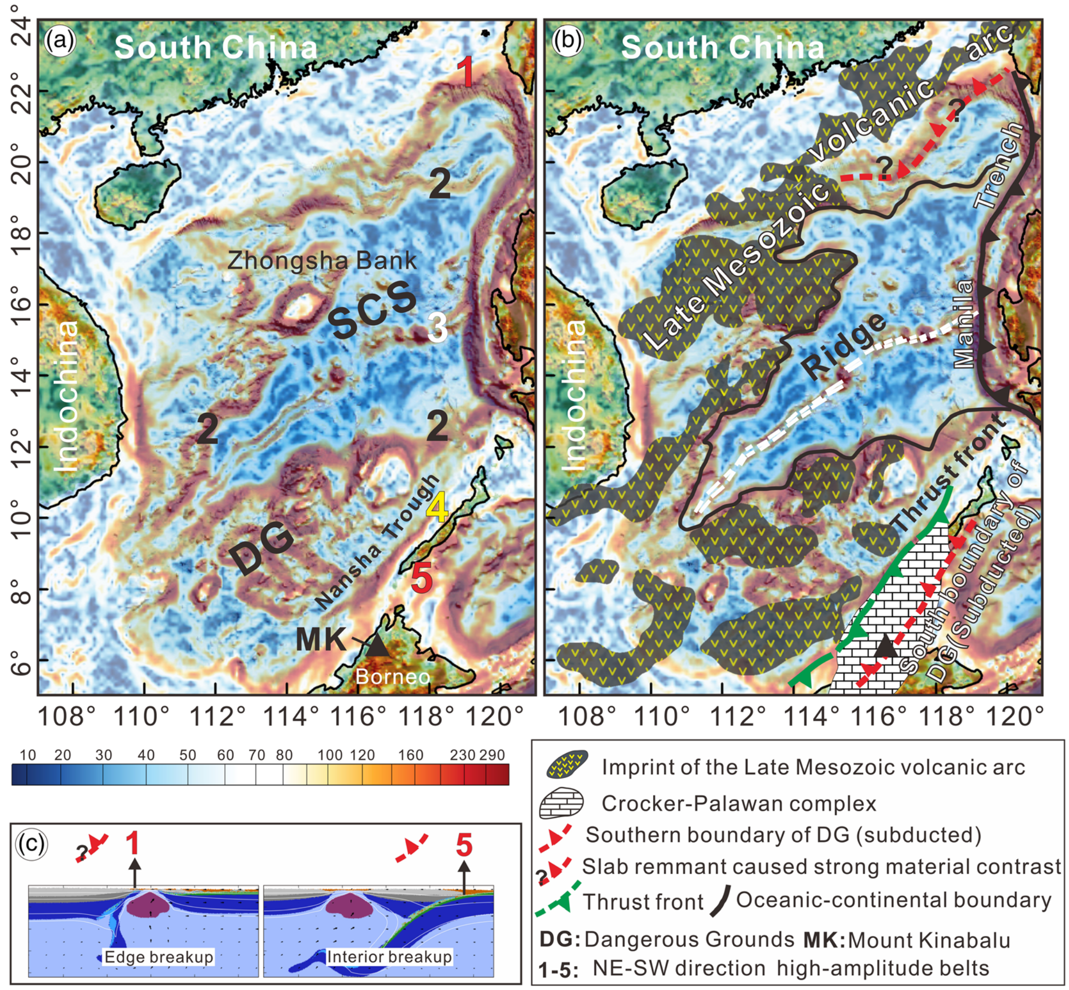

Figure 9. Map of the horizontal gradient of the Bouguer anomaly in the SCS region without (a) and with (b) interpretation and (c) the numerical models used for comparison. High-amplitude anomaly belts paralleling to the South China continental margin are numbered. The region of the Crocker-Palawan complex is modified after Hutchison (2004). The free-air gravity anomaly data are obtained from the satellite-derived field produced by Sandwell et al. (2014). Terrain corrections for Bouguer gravity anomalies are derived from 1′ ×1′ resolution ETOPO1 model (Amante & Eakins, 2009). Nansha Trough (NW Borneo trough), Nansha (Dangerous Grounds).

oceanic crust has been identified in the middle crust from seismic reflections in the northern SCS margin (e.g., Hu et al., 2008; Huang et al., 2005; Zhou et al., 2006). These identified crust remnants coincide with the gravity anomaly belt and thus provide additional support to our interpretation. In conclusion, the opening of the SCS basin has broken the continental interior in the west, moving the west part of the northwest-directed trench (Belt 5) southward to Borneo with the Dangerous Grounds. By contrast, the initial breakup site for the east SCS is the continental edge, and thus, the east part of the northwest-directed trench (Belt 1) remains in the northern SCS margin.

4.4. Model Limitations

Our thermo-mechanical experiments consider the southeastward subduction of the PSCS as the driving force that induces the continental breakup in the context of convergence. However, we only tested the effects of subduction duration and oceanic age. Other factors, such as surface process (e.g., Andres-Martinez et al., 2019; Erdős et al., 2014; Olive et al., 2014), rheological heterogeneities (e.g., Vogt et al., 2017), plate motion direction (Duclaux et al., 2019; Sun et al., 2020), and fluids (Gerya & Meilick, 2011), might have also facilitated this breakup process, but investigating all their contributions are beyond the scope of this study. In the future, the effects of these factors on the evolution of the SCS should be investigated and evaluated.

Our simulations are here simplified using a 2-D process, which does not allow analyzing the 3-D effects. 3-D numerical simulations are necessary tools to investigate the lateral strain propagation during the model's evolution (e.g., Beniest et al., 2017; Koptev et al., 2017; Menant et al., 2016). However, as we focus on evolution from rift initiation to breakup and not on rift propagation, the use of a 2-D setup in our study is meaningful to investigate the conditions of creating a new rifted margin. In addition, the 2-D subduction model can generate large enough mechanical force to break the continent, in accordance with previous works (Leng & Gurnis, 2011; Tan et al., 2012). Although simplified, our present models are applicable to natural examples and thus can provide first-order estimates of continental breakup induced by subduction direction reversal.

5. Conclusions

In this study, we investigate how the subduction direction reversal controls the continental breakup styles using thermo-mechanical modeling based on the available geological and geophysical constraints from the SCS. The results show that the drag force induced by subduction direction reversal can invoke breakup of the South China continent, and two breakup modes, namely, continental interior and continental edge breakup, are developed depending on the slab age and subduction duration. The continental interior breakup mode is characterized by separating a large continental block from the overriding plate. By contrast, the continental edge breakup mode develops a wide zone of less continuous continental fragments and tearing of the subducted slab. For a slab age of ~15 to ~45 Ma, the continental interior breakup mode requires a longer subduction duration than the edge breakup mode. The continental edge breakup always occurs when the slab age is younger than ~15 Ma, whereas the breakup only develops within the interior once the age exceeds ~45 Ma.

By comparing the modeling results to the final rifting characteristics of the SCS, our results suggest that the variation in the subduction duration might be a reason for the contrasting breakup locus along the strike of the SCS margin. That is, the eastern South China margin has experienced a relatively short-period PSCS subduction and thus is characterized by the breakup of the edge region, whereas the western South China margin undergoes a long-period subduction and thus has been broken in the interior region.

A combination of HGBA and numerical modeling suggests that a two-segment northwest-directed trench exists in the present-day SCS region. The western segment has moved southward together with the Dangerous Grounds and now lies beneath the Crocker-Palawan accretionary wedge. The eastern segment is found in the northern SCS margin, extending from the Central Uplift to the Yitongansha.

Acknowledgments

This research was supported by the Guangdong NSF research team project (2017A030312002), the Key Special Project for Introduced Talents Team of Southern Marine Science and Engineering Guangdong Laboratory (Guangzhou) (GML2019ZD0205), the K. C. Wong Education Foundation (GJTD-2018-13), the Strategic Priority Research Program of the Chinese Academy of Science (XDA13010303), the Chinese Academy of Sciences (Y4SL021001, QYZDY-SSWDQC005, 133244KYSB20180029, and ISEE2019ZR01), the NSFC project (41606073, 41890813, and 41576070), the IODP-China Foundation, the OMG Visiting Fellowship (OMG18-15), and the Hong Kong Research Grant Council Grants (Nos. 14313816 and 14304820). We thank Fabio Crameri, Marta Pérez-Gussinyé, two anonymous reviewers, editor Laurent Jolivet, and associated editor Laurent Husson for their constructive comments that contributed to improving the manuscript. An earlier review by Guillaume Duclaux is also appreciated.

Data Availability Statement

Data can be obtained from a repository (https://figshare.com/s/ed3174627a7090e9ad45).

References

Amante, C., & Eakins, B. W. (2009). *ETOPO1 arc-minute global relief model: Procedures, data sources and analysis*.

An, M., & Shi, Y. (2006). Lithospheric thickness of the Chinese continent. *Physics of the Earth and Planetary Interiors*, *159*(3–4), 257–266. https://doi.org/10.1016/j.pepi.2006.08.002

Andres-Martinez, M., Perez-Gussinye, M., Armitage, J., & Morgan, J. P. (2019). Thermomechanical implications of sediment transport for the architecture and evolution of continental rifts and margins. *Tectonics*, *38*, 641–665. https://doi.org/10.1029/2018TC005346

Barckhausen, U., Engels, M., Franke, D., Ladage, S., & Pubellier, M. (2014). Evolution of the South China Sea: Revised ages for breakup and seafloor spreading. *Marine and Petroleum Geology*, *58*, 599–611. https://doi.org/10.1016/j.marpetgeo.2014.02.022

Beaussier, S. J., Gerya, T. V., & Burg, J.-P. (2019). Near-ridge initiation of intraoceanic subduction: Effects of inheritance in 3D numerical models of the Wilson cycle. *Tectonophysics*, *763*, 1–13. https://doi.org/10.1016/j.tecto.2019.04.011

Becker, T., Schaeffer, A., Lebedev, S., & Conrad, C. (2015). Toward a generalized plate motion reference frame. *Geophysical Research Letters*, *42*, 3188–3196. https://doi.org/10.1002/2015GL063695

Behn, M. D., Conrad, C. P., & Silver, P. G. (2004). Detection of upper mantle flow associated with the African Superplume. *Earth and Planetary Science Letters*, *224*(3–4), 259–274. https://doi.org/10.1016/j.epsl.2004.05.026

Beniest, A., Koptev, A., & Burov, E. (2017). Numerical models for continental break-up: Implications for the South Atlantic. *Earth and Planetary Science Letters*, *461*, 176–189. https://doi.org/10.1016/j.epsl.2016.12.034

Bercovici, D. (2003). The generation of plate tectonics from mantle convection. *Earth and Planetary Science Letters*, *205*(3–4), 107–121. https://doi.org/10.1016/S0012-821X(02)01009-9

Briais, A., Patriat, P., & Tapponnier, P. (1993). Updated interpretation of magnetic-anomalies and sea-floor spreading stages in the South China Sea—Implications for the tertiary tectonics of Southeast Asia. *Journal of Geophysical Research*, *98*(B4), 6299–6328. https://doi.org/10.1029/92JB02280

Brune, S., Williams, S. E., Butterworth, N. P., & Müller, R. D. (2016). Abrupt plate accelerations shape rifted continental margins. *Nature*, *536*(7615), 201–204. https://doi.org/10.1038/nature18319

Buck, W. R. (1991). Modes of continental lithospheric extension. *Journal of Geophysical Research*, *96*(B12), 20,161–20,178. https://doi.org/10.1029/91JB01485

Burg, J. P., & Gerya, T. (2005). The role of viscous heating in Barrovian metamorphism of collisional orogens: Thermomechanical models and application to the Lepontine Dome in the Central Alps. *Journal of Metamorphic Geology*, *23*(2), 75–95. https://doi.org/10.1111/j.1525-1314.2005.00563.x

Burov, E., & Watts, A. (2006). The long-term strength of continental lithosphere: "jelly sandwich" or "crème brûlée"? *GSA Today*, *16*(1), 4. https://doi.org/10.1130/1052-5173(2006)016<4:TLTSOC>2.0.CO;2

Cande, S. C., & Stegman, D. R. (2011). Indian and African plate motions driven by the push force of the Réunion plume head. *Nature*, *475*(7354), 47–52. https://doi.org/10.1038/nature10174

Capitanio, F. A., Stegman, D. R., Moresi, L.-N., & Sharples, W. (2010). Upper plate controls on deep subduction, trench migrations and deformations at convergent margins. *Tectonophysics*, *483*(1–2), 80–92. https://doi.org/10.1016/j.tecto.2009.08.020

Chenin, P., Manatschal, G., Picazo, S., Müntener, O., Karner, G., Johnson, C., & Ulrich, M. (2017). Influence of the architecture of magma-poor hyperextended rifted margins on orogens produced by the closure of narrow versus wide oceans. *Geosphere*, *13*(2), 559–576. https://doi.org/10.1130/GES01363.1

Choi, E., Tan, E., Lavier, L. L., & Calo, V. M. (2013). DynEarthSol2D: An efficient unstructured finite element method to study long-term tectonic deformation. *Journal of Geophysical Research: Solid Earth*, *118*, 2429–2444. https://doi.org/10.1002/jgrb.50148

Chopra, P., & Paterson, M. S. (1981). The experimental deformation of dunite. *Tectonophysics*, *78*(1–4), 453–473. https://doi.org/10.1016/0040-1951(81)90024-X

Clift, P., Lee, G. H., Duc, N. A., Barckhausen, U., Long, H. V., & Zhen, S. (2008). Seismic reflection evidence for a Dangerous Grounds miniplate: No extrusion origin for the South China Sea. *Tectonics*, *27*, TC3008. https://doi.org/10.1029/2007TC002216

Coltice, N., Husson, L., Faccenna, C., & Arnould, M. (2019). What drives tectonic plates? *Science Advances*, *5*(10), eaax4295. https://doi.org/10.1126/sciadv.aax4295

Cottam, M., Hall, R., Sperber, C., & Armstrong, R. (2010). Pulsed emplacement of the Mount Kinabalu granite, northern Borneo. *Journal of the Geological Society*, *167*(1), 49–60. https://doi.org/10.1144/0016-76492009-028

Crameri, F., Schmeling, H., Golabek, G., Duretz, T., Orendt, R., Buiter, S., et al. (2012). A comparison of numerical surface topography calculations in geodynamic modelling: An evaluation of the 'sticky air' method. *Geophysical Journal International*, *189*(1), 38–54. https://doi.org/10.1111/j.1365-246X.2012.05388.x

Crameri, F., & Tackley, P. J. (2015). Parameters controlling dynamically self-consistent plate tectonics and single-sided subduction in global models of mantle convection. *Journal of Geophysical Research: Solid Earth*, *120*, 3680–3706. https://doi.org/10.1002/2014JB011664

Cullen, A., Reemst, P., Henstra, G., Gozzard, S., & Ray, A. (2010). Rifting of the South China Sea: New perspectives. *Petroleum Geoscience*, *16*(3), 273–282. https://doi.org/10.1144/1354-079309-908

Dal Zilio, L., Faccenda, M., & Capitanio, F. (2017). The role of deep subduction in supercontinent breakup. *Tectonophysics*, *746*, 312–324.

Ding, W., & Li, J. (2016). Propagated rifting in the Southwest Sub-basin, South China Sea: Insights from analogue modelling. *Journal of Geodynamics*, *100*, 71–86.

Duclaux, G., Huismans, R. S., & May, D. A. (2019). Rotation, narrowing, and preferential reactivation of brittle structures during oblique rifting. *Earth and Planetary Science Letters*, *531*, 115952.

Duretz, T., Petri, B., Mohn, G., Schmalholz, S. M., Schenker, F. L., & Müntener, O. (2016). The importance of structural softening for the evolution and architecture of passive margins. *Scientific Reports*, *6*(1), 38704. https://doi.org/10.1038/srep38704

Durham, W., Mei, S., Kohlstedt, D., Wang, L., & Dixon, N. (2009). New measurements of activation volume in olivine under anhydrous conditions. *Physics of the Earth and Planetary Interiors*, *172*(1–2), 67–73. https://doi.org/10.1016/j.pepi.2008.07.045

Erdős, Z., Huismans, R. S., van der Beek, P., & Thieulot, C. (2014). Extensional inheritance and surface processes as controlling factors of mountain belt structure. *Journal of Geophysical Research: Solid Earth*, *119*, 9042–9061. https://doi.org/10.1002/2014JB011408

Faccenna, C., Holt, A. F., Becker, T. W., Lallemand, S., & Royden, L. H. (2018). Dynamics of the Ryukyu/Izu-Bonin-Marianas double subduction system. *Tectonophysics*, *746*, 229–238. https://doi.org/10.1016/j.tecto.2017.08.011

Fan, J., Zhao, D., Dong, D., & Zhang, G. (2017). P-wave tomography of subduction zones around the central Philippines and its geodynamic implications. *Journal of Asian Earth Sciences*, *146*, 76–89. https://doi.org/10.1016/j.jseaes.2017.05.015

Franke, D., Barckhausen, U., Heyde, I., Tingay, M., & Ramli, N. (2008). Seismic images of a collision zone offshore NW Sabah/Borneo. *Marine and Petroleum Geology*, *25*(7), 606–624. https://doi.org/10.1016/j.marpetgeo.2007.11.004

Franke, D., Savva, D., Pubellier, M., Steuer, S., Mouly, B., Auxietre, J.-L., et al. (2014). The final rifting evolution in the South China Sea. *Marine and Petroleum Geology*, *58*, 704–720. https://doi.org/10.1016/j.marpetgeo.2013.11.020

Gerya, T. (2010). *Introduction to numerical geodynamic modelling*. Cambridge: Cambridge University Press.

Gerya, T. V., & Meilick, F. (2011). Geodynamic regimes of subduction under an active margin: Effects of rheological weakening by fluids and melts. *Journal of Metamorphic Geology*, *29*(1), 7–31. https://doi.org/10.1111/j.1525-1314.2010.00904.x

Gueydan, F., & Précigout, J. (2014). Modes of continental rifting as a function of ductile strain localization in the lithospheric mantle. *Tectonophysics*, *612*, 18–25.

Hall, R. (2002). Cenozoic geological and plate tectonic evolution of SE Asia and the SW Pacific: Computer-based reconstructions, model and animations. *Journal of Asian Earth Sciences*, *20*(4), 353–431. https://doi.org/10.1016/S1367-9120(01)00069-4

Hall, R., & Spakman, W. (2015). Mantle structure and tectonic history of SE Asia. *Tectonophysics*, *658*, 14–45. https://doi.org/10.1016/j.tecto.2015.07.003

Hall, R., van Hattum, M. W., & Spakman, W. (2008). Impact of India-Asia collision on SE Asia: The record in Borneo. *Tectonophysics*, *451*(1–4), 366–389. https://doi.org/10.1016/j.tecto.2007.11.058

Hamilton, W. B. (1979). *Tectonics of the Indonesian region*. Washington, DC: US Government Printing Office.

Heuret, A., & Lallemand, S. (2005). Plate motions, slab dynamics and back-arc deformation. *Physics of the Earth and Planetary Interiors*, *149*(1–2), 31–51. https://doi.org/10.1016/j.pepi.2004.08.022

Holloway, N. (1982). North Palawan block, Philippines—Its relation to Asian mainland and role in evolution of South China Sea. *AAPG Bulletin*, *66*(9), 1355–1383.

Holt, A. F., Royden, L. H., Becker, T. W., & Faccenna, C. (2018). Slab interactions in 3-D subduction settings: The Philippine Sea Plate region. *Earth and Planetary Science Letters*, *489*, 72–83. https://doi.org/10.1016/j.epsl.2018.02.024

Hu, D., Zhou, D., Wu, X., & He, M. (2008). Origin of high magnetic anomaly belt in northeastern South China Sea as indicated by geophysical inversion. *Journal of Tropical Oceanography (in Chinese with English abstract)*, *27*(1), 32–37.

Huang, C., Zhou, D., Sun, Z., Chen, C., & Hao, H. (2005). Deep crustal structure of Baiyun Sag, northern South China Sea revealed from deep seismic reflection profile. *Chinese Science Bulletin*, *50*(11), 1131–1138. https://doi.org/10.1360/04wd0207

Huang, Z., Zhao, D., & Wang, L. (2015). P wave tomography and anisotropy beneath Southeast Asia: Insight into mantle dynamics. *Journal of Geophysical Research: Solid Earth*, *120*, 5154–5174. https://doi.org/10.1002/2015JB012098

Huchon, P., Nguyen, T. N. H., & Chamot-Rooke, N. (2001). Propagation of continental break-up in the southwestern South China Sea. *Non-Volcanic Rifting of Continental Margins: A Comparison of Evidence from Land and Sea*, *187*, 31–50.

Huismans, R. S., & Beaumont, C. (2003). Symmetric and asymmetric lithospheric extension: Relative effects of frictional-plastic and viscous strain softening. *Journal of Geophysical Research*, *108*(B10), 2496. https://doi.org/10.1029/2002JB002026

Husson, L. (2012). Trench migration and upper plate strain over a convecting mantle. *Physics of the Earth and Planetary Interiors*, *212*, 32–43.

Hutchison, C. S. (1996). The 'Rajang accretionary prism' and 'Lupar Line' problem of Borneo. *Geological Society, London, Special Publications*, *106*(1), 247–261. https://doi.org/10.1144/GSL.SP.1996.106.01.16

Hutchison, C. S. (2004). Marginal basin evolution: The southern South China Sea. *Marine and Petroleum Geology*, *21*(9), 1129–1148. https://doi.org/10.1016/j.marpetgeo.2004.07.002

Hutchison, C. S., & Vijayan, V. (2010). What are the Spratly Islands? *Journal of Asian Earth Sciences*, *39*(5), 371–385. https://doi.org/10.1016/j.jseaes.2010.04.013

Isozaki, Y. (1988). Permian, Triassic and Jurassic bedded radiolarian cherts in North Palawan Block, Philippines: Evidence of late Mesozoic subduction-accretion, Rep. No. 3 IGCP Proj. 224: Pre-Jurassic Evolution of Eastern Asia, 99–115.

Jolivet, L., Faccenna, C., Becker, T., Tesauro, M., Sternai, P., & Bouilhol, P. (2018). Mantle flow and deforming continents: From India-Asia convergence to Pacific subduction. *Tectonics*, *37*, 2887–2914. https://doi.org/10.1029/2018TC005036

Jourdon, A., Le Pourhiet, L., Mouthereau, F., & Masini, E. (2019). Role of rift maturity on the architecture and shortening distribution in mountain belts. *Earth and Planetary Science Letters*, *512*, 89–99. https://doi.org/10.1016/j.epsl.2019.01.057

Karato, S.-I., & Wu, P. (1993). Rheology of the upper mantle: A synthesis. *Science*, *260*(5109), 771–778. https://doi.org/10.1126/science.260.5109.771

Karig, D. E. (1971). Origin and development of marginal basins in the western Pacific. *Journal of Geophysical Research*, *76*(11), 2542–2561. https://doi.org/10.1029/JB076i011p02542

Keppie, D. F., Currie, C. A., & Warren, C. (2009). Subduction erosion modes: Comparing finite element numerical models with the geological record. *Earth and Planetary Science Letters*, *287*(1–2), 241–254. https://doi.org/10.1016/j.epsl.2009.08.009

Kirby, S. H. (1983). Rheology of the lithosphere. *Reviews of Geophysics*, *21*(6), 1458–1487. https://doi.org/10.1029/RG021i006p01458

Koptev, A., Beniest, A., Gerya, T., Ehlers, T. A., & Jolivet, L. (2019). Plume-induced breakup of a subducting plate: Microcontinent formation without cessation of the subduction process. *Geophysical Research Letters*, *46*, 3663–3675. https://doi.org/10.1029/2018GL081295

Koptev, A., Burov, E., Gerya, T., le Pourhiet, L., Leroy, S., Calais, E., & Jolivet, L. (2017). Plume-induced continental rifting and break-up in ultra-slow extension context: Insights from 3D numerical modeling. *Tectonophysics*, *746*, 121–137.

Koptev, A., Calais, E., Burov, E., Leroy, S., & Gerya, T. (2015). Dual continental rift systems generated by plume-lithosphere interaction. *Nature Geoscience*, *8*(5), 388–392. https://doi.org/10.1038/ngeo2401

Lallemand, S., Heuret, A., & Boutelier, D. (2005). On the relationships between slab dip, back-arc stress, upper plate absolute motion, and crustal nature in subduction zones. *Geochemistry, Geophysics, Geosystems*, *6*, Q09006. https://doi.org/10.1029/2005GC000917

Lavier, L. L., & Manatschal, G. (2006). A mechanism to thin the continental lithosphere at magma-poor margins. *Nature*, *440*(7082), 324–328. https://doi.org/10.1038/nature04608

Le Pourhiet, L., Chamot-Rooke, N., Delescluse, M., May, D. A., Watremez, L., & Pubellier, M. (2018). Continental break-up of the South China Sea stalled by far-field compression. *Nature Geoscience*, *11*(8), 605–609. https://doi.org/10.1038/s41561-018-0178-5

Leng, W., & Gurnis, M. (2011). Dynamics of subduction initiation with different evolutionary pathways. *Geochemistry, Geophysics, Geosystems*, *12*, Q12018. https://doi.org/10.1029/2011GC003877

Li, C.-F., Xu, X., Lin, J., Sun, Z., Zhu, J., Yao, Y., et al. (2014). Ages and magnetic structures of the South China Sea constrained by deep tow magnetic surveys and IODP Expedition 349. *Geochemistry, Geophysics, Geosystems*, *15*, 4958–4983. https://doi.org/10.1002/2014GC005567

Li, F., Sun, Z., Pang, X., Liao, J., Yang, H., Xie, H., et al. (2019). Low-viscosity crustal layer controls the crustal architecture and thermal distribution at hyper-extended margins: Modeling insight and application to the northern South China Sea margin. *Geochemistry, Geophysics, Geosystems*, *20*, 3248–3267. https://doi.org/10.1029/2019GC008200

Li, F., Sun, Z., & Yang, H. (2018). Possible spatial distribution of the Mesozoic volcanic arc in the present-day South China Sea continental margin and its tectonic implications. *Journal of Geophysical Research: Solid Earth*, *123*, 6215–6235. https://doi.org/10.1029/2017JB014861

Li, F., Sun, Z., & Zhang, J. (2018). Numerical studies on continental lithospheric breakup in response to the extension induced by subduction direction inversion. *Earth Science (In Chinese with English abstract)*, *43*(10), 3762–3777.

Li, J., Ding, W., Wu, Z., Zhang, J., & Dong, C. (2012). The propagation of seafloor spreading in the southwestern subbasin, South China Sea. *Chinese Science Bulletin*, *57*(24), 3182–3191. https://doi.org/10.1007/s11434-012-5329-2

Li, S., Suo, Y., Li, X., Zhou, J., Santosh, M., & Wang, P. (2019). Mesozoic tectono-magmatic response in the East Asian ocean-continent connection zone to subduction of the Paleo-Pacific Plate. *Earth-Science Reviews*, *192*, 91–137. https://doi.org/10.1016/j.earscirev.2019.03.003

Li, Z., & Li, X. (2007). Formation of the 1300-km-wide intracontinental orogen and postorogenic magmatic province in Mesozoic South China: A flat-slab subduction model. *Geology*, *35*(2), 179–182. https://doi.org/10.1130/G23193A.1

Liao, J., & Gerya, T. (2017). Partitioning of crustal shortening during continental collision: 2-D thermomechanical modeling. *Journal of Geophysical Research: Solid Earth*, *122*, 592–606. https://doi.org/10.1002/2016JB013398

Liao, J., Gerya, T., & Wang, Q. (2013). Layered structure of the lithospheric mantle changes dynamics of craton extension. *Geophysical Research Letters*, *40*, 5861–5866. https://doi.org/10.1002/2013GL058081

Madon, M., Kim, C. L., & Wong, R. (2013). The structure and stratigraphy of deepwater Sarawak, Malaysia: Implications for tectonic evolution. *Journal of Asian Earth Sciences*, *76*, 312–333.

Marotta, A. M., Spalla, M. I., & Gosso, G. (2009). Upper and lower crustal evolution during lithospheric extension: Numerical modelling and natural footprints from the European Alps. *Geological Society of London, Special Publication*, *321*(1), 33–72. https://doi.org/10.1144/SP321.3

Marquez, E. J., Aitchison, J. C., & Zamoras, L. R. (2006). Upper Permian to Middle Jurassic radiolarian assemblages of Busuanga and surrounding islands, Palawan, Philippines. *Eclogae Geologicae Helvetiae*, *99*(S1), S101–S125. https://doi.org/10.1007/s00015-006-0606-1

Maruyama, S., Isozaki, Y., Kimura, G., & Terabayashi, M. (1997). Paleogeographic maps of the Japanese Islands: Plate tectonic synthesis from 750 Ma to the present. *Island Arc*, *6*(1), 121–142. https://doi.org/10.1111/j.1440-1738.1997.tb00043.x
Menant, A., Sternai, P., Jolivet, L., Guillou-Frottier, L., & Gerya, T. (2016). 3D numerical modeling of mantle flow, crustal dynamics and magma genesis associated with slab roll-back and tearing: The eastern Mediterranean case. *Earth and Planetary Science Letters*, *442*, 93–107. https://doi.org/10.1016/j.epsl.2016.03.002
Mishin, Y. A., Gerya, T. V., Burg, J.-P., & Connolly, J. A. (2008). Dynamics of double subduction: Numerical modeling. *Physics of the Earth and Planetary Interiors*, *171*(1–4), 280–295. https://doi.org/10.1016/j.pepi.2008.06.012
Mohn, G., Manatschal, G., Beltrando, M., Masini, E., & Kusznir, N. (2012). Necking of continental crust in magma-poor rifted margins: Evidence from the fossil Alpine Tethys margins. *Tectonics*, *31*, TC1012. https://doi.org/10.1029/2011TC002961
Mondy, L. S., Rey, P. F., Duclaux, G., & Moresi, L. (2018). The role of asthenospheric flow during rift propagation and breakup. *Geology*, *46*(2), 103–106. https://doi.org/10.1130/G39674.1
Naliboff, J. B., Buiter, S. J. H., Péron-Pinvidic, G., Osmundsen, P. T., & Tetreault, J. (2017). Complex fault interaction controls continental rifting. *Nature Communications*, *8*(1), 1179. https://doi.org/10.1038/s41467-017-00904-x
Nemčok, M., Stuart, C., Rosendahl, B., Welker, C., Smith, S., Sheya, C., et al. (2013). Continental break-up mechanism; lessons from intermediate-and fast-extension settings. *Geological Society, London, Special Publications*, *369*(1), 373–401. https://doi.org/10.1144/SP369.14
Nirrengarten, M., Manatschal, G., Tugend, J., Kusznir, N., & Sauter, D. (2018). Kinematic evolution of the southern North Atlantic: Implications for the formation of hyperextended rift systems. *Tectonics*, *37*, 89–118. https://doi.org/10.1002/2017TC004495
Nissen, S. S., Hayes, D. E., Buhl, P., Diebold, J., Bochu, Y., Zeng, W., & Chen, Y. (1995). Deep penetration seismic soundings across the northern margin of the South China Sea. *Journal of Geophysical Research*, *100*(B11), 22,407–22,433. https://doi.org/10.1029/95JB01866
Olive, J. A., Behn, M. D., & Malatesta, L. C. (2014). Modes of extensional faulting controlled by surface processes. *Geophysical Research Letters*, *41*, 6725–6733. https://doi.org/10.1002/2014GL061507
Pautot, G., Rangin, C., Briais, A., Tapponnier, P., Beuzart, P., Lericolais, G., et al. (1986). Spreading direction in the central South China Sea.
Pérez-Gussinyé, M., Morgan, J. P., Reston, T. J., & Ranero, C. R. (2006). The rift to drift transition at non-volcanic margins: Insights from numerical modelling. *Earth and Planetary Science Letters*, *244*(1–2), 458–473. https://doi.org/10.1016/j.epsl.2006.01.059
Pérez-Gussinyé, M., Ranero, C. R., Reston, T. J., & Sawyer, D. (2003). Mechanisms of extension at nonvolcanic margins: Evidence from the Galicia interior basin, west of Iberia. *Journal of Geophysical Research*, *108*(B5), 2245. https://doi.org/10.1029/2001JB000901
Péron-Pinvidic, G., & Manatschal, G. (2009). The final rifting evolution at deep magma-poor passive margins from Iberia-Newfoundland: A new point of view. *International Journal of Earth Sciences*, *98*(7), 1581–1597. https://doi.org/10.1007/s00531-008-0337-9
Phillips, B. R., & Bunge, H.-P. (2005). Heterogeneity and time dependence in 3D spherical mantle convection models with continental drift. *Earth and Planetary Science Letters*, *233*(1–2), 121–135. https://doi.org/10.1016/j.epsl.2005.01.041
Qiu, X., Zhao, M., Ao, W., Lü, C., Hao, T., You, Q., et al. (2011). OBS survey and crustal structure of the SW Sub-Basin and Nansha Block, South China Sea. *Chinese Journal of Geophysics*, *54*(6), 1009–1021. https://doi.org/10.1002/cjg2.1680
Ranalli, G. (1995). *Rheology of the Earth*. New York: Springer Science & Business Media.
Ranalli, G., & Murphy, D. C. (1987). Rheological stratification of the lithosphere. *Tectonophysics*, *132*(4), 281–295. https://doi.org/10.1016/0040-1951(87)90348-9
Rodríguez-González, J., Negredo, A. M., & Billen, M. I. (2012). The role of the overriding plate thermal state on slab dip variability and on the occurrence of flat subduction. *Geochemistry, Geophysics, Geosystems*, *13*, Q01002. https://doi.org/10.1029/2011GC003859
Ros, E., Perez-Gussinye, M., Araujo, M., Romeiro, M. T., Andres-Martinez, M., & Morgan, J. P. (2017). Lower crustal strength controls on melting and serpentinization at magma-poor margins: Potential implications for the South Atlantic. *Geochemistry, Geophysics, Geosystems*, *18*, 4538–4557. https://doi.org/10.1002/2017GC007212
Sandwell, D. T., Müller, R. D., Smith, W. H., Garcia, E., & Francis, R. (2014). New global marine gravity model from CryoSat-2 and Jason-1 reveals buried tectonic structure. *Science*, *346*(6205), 65–67. https://doi.org/10.1126/science.1258213
Sdrolias, M., & Muller, R. D. (2006). Controls on back-arc basin formation. *Geochemistry, Geophysics, Geosystems*, *7*, Q04016. https://doi.org/10.1029/2005GC001090
Shelton, G. L., Tullis, J., & Tullis, T. (1981). Experimental high temperature and high pressure faults. *Geophysical Research Letters*, *8*(1), 55–58. https://doi.org/10.1029/GL008i001p00055
Stern, R. J. (2002). Subduction zones. *Reviews of Geophysics*, *40*(4), 1012. https://doi.org/10.1029/2001RG000108
Steuer, S., Franke, D., Meresse, F., Savva, D., Pubellier, M., Auxietre, J.-L., & Aurelio, M. (2013). Time constraints on the evolution of southern Palawan Island, Philippines from onshore and offshore correlation of Miocene limestones. *Journal of Asian Earth Sciences*, *76*, 412–427.
Sun, W., Zhang, L., Liao, R., Sun, S., Li, C., & Liu, H. (2020). Plate convergence in the Indo-Pacific region. *Journal of Oceanology and Limnology*, *38*(4), 1008–1017. https://doi.org/10.1007/s00343-020-0146-y
Sun, Z., Lin, J., Qiu, N., Jian, Z., Wang, P., Pang, X., et al. (2019). The role of magmatism in thinning and breakup of the South China Sea continental margin. *National Science Review*, *6*(5), 871–876. https://doi.org/10.1093/nsr/nwz116
Sun, Z., Zhong, Z., Keep, M., Zhou, D., Cai, D., Li, X., et al. (2009). 3D analogue modeling of the South China Sea: A discussion on breakup pattern. *Journal of Asian Earth Sciences*, *34*(4), 544–556. https://doi.org/10.1016/j.jseaes.2008.09.002
Svartman Dias, A. E., Lavier, L. L., & Hayman, N. W. (2015). Conjugate rifted margins width and asymmetry: The interplay between lithospheric strength and thermomechanical processes. *Journal of Geophysical Research: Solid Earth*, *120*, 8672–8700. https://doi.org/10.1002/2015JB012074
Tan, E., Lavier, L. L., Avendonk, H. J. A. V., & Heuret, A. (2012). The role of frictional strength on plate coupling at the subduction interface. *Geochemistry, Geophysics, Geosystems*, *13*, Q10006. https://doi.org/10.1029/2012GC004214
Taylor, B., & Hayes, D. E. (1983). Origin and history of the South China Sea basin, The tectonic and geologic evolution of Southeast Asian seas and islands: Part 2. *GMS*, *27*, 23–56.
Tetreault, J., & Buiter, S. (2018). The influence of extension rate and crustal rheology on the evolution of passive margins from rifting to break-up. *Tectonophysics*, *746*, 155–172. https://doi.org/10.1016/j.tecto.2017.08.029
Tumanda, F. (1991). Radiolarian biostratigraphy in central Busuanga Island, Palawan, Philippines. *Journal of the Geological Society of the Philippines*, *46*, 49–104.
Turcotte, D. L., Emerman, S. H., Morgan, P., & Baker, B. H. (1983). Mechanisms of active and passive rifting. *Tectonophysics*, *94*(1–4), 39–50. https://doi.org/10.1016/0040-1951(83)90008-2
Turcotte, D. L., & Schubert, G. (2002). *Geodynamics*. Cambridge: Cambridge university press.
Vermeer, P. (1990). The orientation of shear bands in biaxial tests. *Geotechnique*, *40*(2), 223–236. https://doi.org/10.1680/geot.1990.40.2.223

Vogt, K., Matenco, L., & Cloetingh, S. (2017). Crustal mechanics control the geometry of mountain belts. Insights from numerical modelling. *Earth and Planetary Science Letters*, *460*, 12–21. https://doi.org/10.1016/j.epsl.2016.11.016

Von Huene, R., & Scholl, D. W. (1991). Observations at convergent margins concerning sediment subduction, subduction erosion, and the growth of continental crust. *Reviews of Geophysics*, *29*(3), 279–316. https://doi.org/10.1029/91RG00969

Wang, P., Huang, C. Y., Lin, J., Jian, Z., Sun, Z., & Zhao, M. (2019). The South China Sea is not a mini-Atlantic: Plate-edge rifting vs intraplate rifting. *National Science Review*, *6*(5), 902–913. https://doi.org/10.1093/nsr/nwz135

Wei, X. D., Ruan, A. G., Zhao, M. H., Qiu, X. L., Li, J. B., Zhu, J. J., & Ding, W. W. (2011). A wide-angle obs profile across the Dongsha uplift and Chaoshan depression in the mid-northern South China Sea. *Chinese Journal of Geophysics*, *54*(6), 1149–1160.

Wolf, S. G., & Huismans, R. S. (2019). Mountain building or Backarc extension in ocean-continent subduction systems: A function of backarc lithospheric strength and absolute plate velocities. *Journal of Geophysical Research: Solid Earth*, *124*, 7461–7482. https://doi.org/10.1029/2018JB017171

Wu, J., & Suppe, J. (2018). Proto-South China Sea plate tectonics using subducted slab constraints from tomography. *Journal of Earth Science*, *29*(6), 1304–1318. https://doi.org/10.1007/s12583-017-0813-x

Xia, S., & Zhao, D. (2014). Late Mesozoic magmatic plumbing system in the onshore-offshore area of Hong Kong: Insight from 3-D active-source seismic tomography. *Journal of Asian Earth Sciences*, *96*, 46–58. https://doi.org/10.1016/j.jseaes.2014.08.038

Xu, C., Shi, H., Barnes, C. G., & Zhou, Z. (2016). Tracing a late Mesozoic magmatic arc along the Southeast Asian margin from the granitoids drilled from the northern South China Sea. *International Geology Review*, *58*(1), 71–94. https://doi.org/10.1080/00206814.2015.1056256

Yamato, P., Husson, L., Becker, T. W., & Pedoja, K. (2013). Passive margins getting squeezed in the mantle convection vice. *Tectonics*, *32*, 1559–1570. https://doi.org/10.1002/2013TC003375

Ye, Q., Mei, L., Shi, H., Shu, Y., Camanni, G., & Wu, J. (2018). A low-angle normal fault and basement structures within the Enping Sag, Pearl River Mouth Basin: Insights into late Mesozoic to early Cenozoic tectonic evolution of the South China Sea area. *Tectonophysics*, *731*, 1–16.

Yoshida, M., & Hamano, Y. (2015). Pangea breakup and northward drift of the Indian subcontinent reproduced by a numerical model of mantle convection. *Scientific Reports*, *5*(1), 8407. https://doi.org/10.1038/srep08407

Zahirovic, S., Matthews, K. J., Flament, N., Müller, R. D., Hill, K. C., Seton, M., & Gurnis, M. (2016). Tectonic evolution and deep mantle structure of the eastern Tethys since the latest Jurassic. *Earth-Science Reviews*, *162*, 293–337. https://doi.org/10.1016/j.earscirev.2016.09.005

Zamoras, L. R., & Matsuoka, A. (2004). Accretion and postaccretion tectonics of the Calamian Islands, North Palawan block, Philippines. *Island Arc*, *13*(4), 506–519. https://doi.org/10.1111/j.1440-1738.2004.00443.x

Zhang, C., Manatschal, G., Pang, X., Sun, Z., Zheng, J., Li, H., et al. (2020). Discovery of Mega-Sheath Folds Flooring the Liwan Subbasin (South China Sea): Implications for the Rheology of Hyperextended Crust. *Geochemistry, Geophysics, Geosystems*, *21*, e2020GC009023. https://doi.org/10.1029/2020gc009023

Zhao, F., Alves, T. M., Xia, S., Li, W., Wang, L., Mi, L., et al. (2020). Along-strike segmentation of the South China Sea margin imposed by inherited pre-rift basement structures. *Earth and Planetary Science Letters*, *530*, 115862. https://doi.org/10.1016/j.epsl.2019.115862

Zhao, M., Qiu, X., Xia, S., Xu, H., Wang, P., Wang, T. K., & Xia, K. (2010). Seismic structure in the northeastern South China Sea: S-wave velocity and Vp/Vs ratios derived from three-component OBS data. *Tectonophysics*, *480*(1–4), 183–197. https://doi.org/10.1016/j.tecto.2009.10.004

Zhou, D., Sun, Z., & Chen, H. (2005). Mesozoic lithofacies, paleo-geography, and tectonic evolution of the South China Sea and surrounding areas. *Earth Science Frontiers*, *12*(3), 204.

Zhou, D., Sun, Z., Chen, H.-z., Xu, H.-h., Wang, W.-y., Pang, X., et al. (2008). Mesozoic paleogeography and tectonic evolution of South China Sea and adjacent areas in the context of Tethyan and Paleo-Pacific interconnections. *Island Arc*, *17*(2), 186–207. https://doi.org/10.1111/j.1440-1738.2008.00611.x

Zhou, D., Wang, W., Wang, J., Pang, X., Cai, D., & Sun, Z. (2006). Mesozoic subduction-accretion zone in northeastern South China Sea inferred from geophysical interpretations. *Science in China Series D*, *49*(5), 471–482. https://doi.org/10.1007/s11430-006-0471-9

Zhu, G., Yang, H., Lin, J., Zhou, Z., Xu, M., Sun, J., & Wan, K. (2019). Along-strike variation in slab geometry at the southern Mariana subduction zone revealed by seismicity through ocean bottom seismic experiments. *Geophysical Journal International*, *218*(3), 2122–2135. https://doi.org/10.1093/gji/ggz272